

Novel Concepts for Integrating the Electric Drive and Auxiliary Dc-Dc Converter for Hybrid Vehicles

H. Plesko¹⁾, J. Biela¹⁾, J. Luomi²⁾, J. W. Kolar¹⁾

¹⁾Power Electronic Systems Laboratory
 Swiss Federal Institute of Technology (ETH)
 ETH Zentrum, ETL/H23
 8092 Zurich, Switzerland
 Email: plesko@lem.ee.ethz.ch

²⁾Power Electronics Laboratory
 Helsinki University of Technology
 P.O. Box 3000, FI-02015 TKK, Finland
 Email: luomi@lem.ee.ethz.ch

Abstract—Cost, volume and weight are three major driving forces in the automotive area. This is also true for hybrid vehicles which attract more and more attention due to increasing fuel costs and air pollution.

In hybrid vehicles the energy distribution system causes a significant share of the volume and the costs. In order to reduce the costs and the volume of this system two new concepts for integrating the dc-dc converter, which transfers the power between the low and the high voltage bus, functionally in the inverter/drive system are presented in this paper. These concepts are verified by simulations and experimental results.

I. INTRODUCTION

Growing fuel costs are just one factor that push the development of hybrid vehicles. Today, there are many car manufacturers that produce hybrid vehicles and the research activities are growing. Figure 1 shows common voltage levels and interconnections for the electric power system of a hybrid vehicle.

Conventional Hybrid Electric Vehicles usually have two different voltage levels. The 14 V dc bus is often supplied by a 12 V battery over a battery charge/discharge unit. Traditional loads such as a heater and lighting systems are connected to this low voltage bus. In addition, there is a high voltage 200 V...600 V dc bus which provides the necessary power for the propulsion system and which is connected to the low voltage bus via a bidirectional dc-dc converter. This converter needs to be galvanically isolated for safety reasons. The machine voltages are produced through a dc-ac converter connected to the high voltage bus.

In recent years, the growing number of additional electrical loads forced the car industry to think about the introduction of an additional 42 V dc bus powered by a 36 V battery. There are other popular possibilities. The high voltage level could be

omitted and the propulsion system could be supplied with 42 V. In [1] this system is compared to the conventional variant. As the advantages of the high voltage solution outweigh that of the low voltage variant, it is assumed in the following that the propulsion system is fed via a high voltage bus.

In order to reduce the costs of the electric system and increase the power density the dc-dc converter, linking the low and the high voltage bus, and the inverter system could be functionally integrated into the inverter/machine. For example, in [2] a possible integration of the dc-dc converter in the inverter system is presented, which is, however, not galvanically isolated.

In [2] a galvanic isolation is not required since the high voltage bar is omitted and the rotating system is fed from 42 V. The zero-sequence voltage at the machine's star point is used to bidirectionally transfer power between the high and the low voltage dc bus. The output voltage is controlled by choosing an appropriate switching scheme. Connecting the zero-sequence system, the inverter operates as a buck-boost converter and the machine's zero-sequence inductance serves as the buck-boost inductor.

There are similar concepts without galvanic isolation presented in [3], [4], [5] and [6].

As mentioned above, it would be desirable to feed the propulsion system from the high voltage bus. The concept proposed in [2] cannot be used here because the high voltage to low voltage converter needs to have a galvanic isolation for safety reasons. In addition the output voltage V_{out} of the dc-dc converter cannot be controlled in every operation region of the drive system. If the inverter operates for example in the six-step mode, the switching state of the inverter is totally determined. There is no degree of freedom to control the

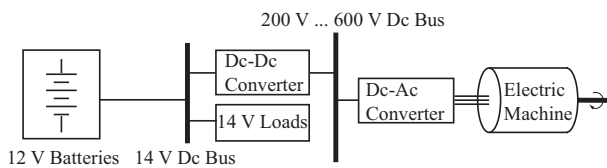


Figure 1: One possibility of a conventional electrical power distribution system architecture for hybrid-electric vehicles.

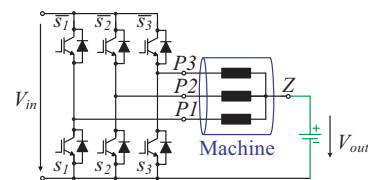


Figure 2: Concept of integration without isolation

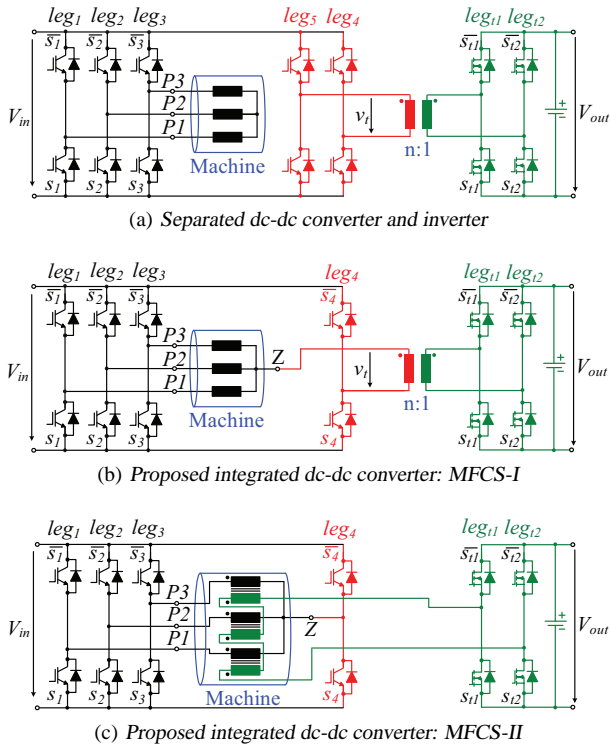


Figure 3: Multi Functional Converter Systems (MFCS).

output voltage. To overcome these problems an integrated high voltage to low voltage dc-dc converter with galvanic isolation is proposed in this paper. Depending on the actual distribution system this converter can be used to convert 200...600 V to 14 V or 42 V.

The starting point for the following considerations is a conventional full bridge converter feeding a high frequency transformer (see figure 3a), whose high frequency output is rectified to the output voltage V_{out} . The secondary side rectifier could be a conventional full bridge configuration or a diode rectifier.

In a first step, the fifth leg (leg_5 in figure 3a) of the conventional system is replaced by the zero-sequence voltage. The transformer is thereby connected to the star point and the midpoint of the primary side leg four (see figure 3b). This concept is referred to as Multi Functional Converter System I (MFCS-I) [9].

In a second step the motor's iron could be used for integrating the transformer as shown in figure 3c. This concept is referred to as Multi Functional Converter System II (MFCS-II) [10]. Other possibilities to use the motor's iron or the input inverter to integrate the transformer are presented in [7] and [8], but the proposed concept saves space because it does not need a three phase rectifier.

In this paper, the basic functions of these two concepts are explained and it will be shown by simulations and experimental results that these concepts work well. The first variant, the multi functional converter system I (MFCS-I), is discussed in **section II**. In **subsection IIA** the basic operation principle for

the MFCS-I is explained, followed by a detailed mathematical flux analysis in **subsection IIB**. The theoretical results will be verified experimentally by means of a 3 kW prototype in **subsection IIC**. In **section III** the results for the MFCS-II are presented. Finally, a conclusion is given in **section IV**.

II. MFCS-I

In the MFCS-I the transformer is connected to the star point and the output of the fourth leg (leg_4 , see figure 3b) thus eliminating one leg of the full bridge compared to the conventional system.

This section starts with an explanation of the basic operation principle of the MFCS-I in **subsection IIA** by studying the zero phase voltage and introducing an equivalent circuit for the dc-dc converter. After discussing the control in **subsection IIB**, the flux is analyzed in detail in **subsection IIC**.

A. Basic Principle of Operation – MFCS-I

Both concepts are based on the utilization of the zero-sequence voltage whose definition and calculation are summarized before the details of the concepts are explained. The zero-phase voltage of a three phase system is defined as

$$v_z = \frac{1}{3}(v_{P1} + v_{P2} + v_{P3}), \quad (1)$$

where v_{P1} , v_{P2} and v_{P3} are the voltages applied to the machine. Depending on the switching state of the inverter, the zero-sequence voltage related to the negative bus bar can be calculated as

$$v_z = \frac{V_{in}}{3}(on_1 + on_2 + on_3), \quad (2)$$

where on_1 is '1' if s_1 is open and $\overline{s_1}$ closed, or else '0'.

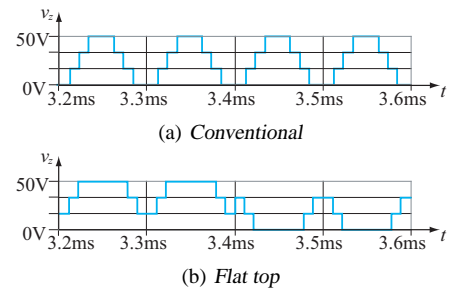


Figure 4: Simulation of the zero-sequence voltage for $M = 0.5$, $f = 10$ kHz and $V_{in} = 50$ V for (a) conventional and (b) flat top modulation.

Figure 4a shows the characteristic of the zero-sequence voltage for the conventional modulation, where the modulation signals are

$$m_{P1}(t) = M \cos(\omega t) - \frac{M}{6} \cos(3\omega t) \quad (3)$$

with $V_{in} = 50$ V and a modulation index $M = 0.5$. The simulation was repeated for the flat top modulation, where the phase with the highest absolute current value is clamped to the positive bus bar if this current is positive, else to the negative (see figure 4b).

The fourth leg (leg_4 , see figure 3b) is required because the zero-sequence voltage remains constant if the inverter operates in six-step mode. Thus, an alternating voltage across the transformer can only be achieved by proper pulsing of s_4 and $\overline{s_4}$.

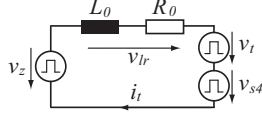


Figure 5: Equivalent circuit for the dc-dc converter.

For the dc-dc converter, the only important part of the inverter-machine subsystem is the zero-sequence voltage v_z , which can be calculated by (2). Thus, the integrated dc-dc converter can be modelled as shown in figure 5. The time dependent voltage source v_z represents the zero-sequence voltage and v_{s4} describes the voltage across s_{s4} (see figure 3b). These two voltage sources are connected to an LR circuit, modelling the machine's zero sequence impedance. v_t represents the transformer voltage (see figure 3b).

It has to be mentioned that v_z , as it is defined in (2), can only be measured if no zero sequence current flows, otherwise it is an analytical parameter. The voltage measured between the star point and the negative bus bar is equivalent to $v_z - v_{lr}$.

This system is similar to a full bridge - rectifier system, but as the voltage v_z applied to the system is neither average free (related to the switching frequency) nor free from even harmonics, a conventional modulation scheme cannot be adopted.

In the actual implementation an active rectifier is used to guarantee that the voltage time product across the transformer remains below a predetermined level. The described dc-dc converter is similar to a dual active bridge [11].

B. Control of MFCS-I

In the further discussion it is without loss of generality assumed, that the motor is driven with space vector modulation. Neglecting the required dead time, there is always one switch of the leg closed.

It is clear that the switching period average of the zero sequence voltage is not always $\frac{V_{in}}{2}$ related to the negative bus bar but may depend on ωt , which is equivalent to the motor's angle. It can be calculated as

$$v_{z_{avg}} = \frac{U_1}{3}(\delta_{P1} + \delta_{P2} + \delta_{P3}), \quad (4)$$

where δ_{P1} is the relative off time of s_1 etc. depending on the motor's angle and the actual modulation factor. To avoid saturation of the transformer, it is necessary that the applied voltage does not show a local average value. This means for the fourth leg that the relative off time δ_{s4} of s_{s4} is determined by the zero sequence voltage as

$$\delta_{s4} = \frac{1}{3}(\delta_{P1} + \delta_{P2} + \delta_{P3}). \quad (5)$$

The only degree of freedom is the relative time offset between the zero phase voltage and the fourth leg voltage, represented through the angle φ_{s4} (see figure 6).

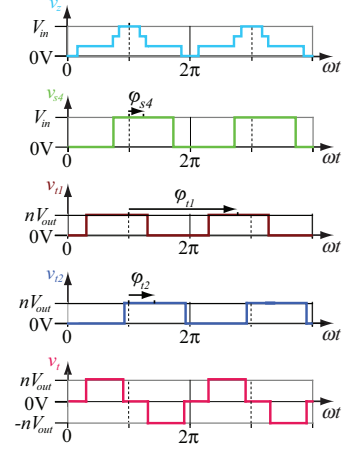


Figure 6: Converter waveforms: zero sequence voltage v_z , voltage v_{s4} across s_4 , voltage v_{t1} across s_{t1} , voltage v_{t2} across s_{t2} and transformer voltage v_t

Further the voltage on the other side of the transformer has to be average free which means that the relative on time of s_{t1} and s_{t2} is 50 percent in stationary operation. The angular offset of the voltage v_{t1} across s_{t1} is called φ_{t1} and the offset of the voltage v_{t2} across s_{t2} is called φ_{t2} .

The Fourier series of the three voltages for the switching frequency f_s can be described as

$$\begin{aligned} v_z &= a_{z(0)} + \sum_{i=1}^{\infty} a_{z(i)} \cos(i\omega_s t) \\ v_{s4} &= a_{s4(0)} + \sum_{i=1}^{\infty} a_{s4(i)} \cos(i\omega_s t - \varphi_{s4}) \\ v_t &= \sum_{i=1}^{\infty} a_{t(i)} [\cos(i\omega_s t - \varphi_{t1}) - \cos(i\omega_s t - \varphi_{t2})] \end{aligned} \quad (6)$$

with $\omega_s = 2\pi f_s$ and

$$\begin{aligned} a_{z(i)} &= \begin{cases} -\frac{2V_{in}}{3i\pi} [\sin(i\pi\delta_a) + \sin(i\pi\delta_b) + \sin(i\pi\delta_c)] & \text{if } i \text{ odd} \\ \frac{2V_{in}}{3i\pi} [\sin(i\pi\delta_a) + \sin(i\pi\delta_b) + \sin(i\pi\delta_c)] & \text{if } i \text{ even} \end{cases} \\ a_{s4(i)} &= \begin{cases} -\frac{2V_{in}}{i\pi} \sin(i\pi\delta_{s4}) & \text{if } i \text{ odd} \\ \frac{2V_{in}}{i\pi} \sin(i\pi\delta_{s4}) & \text{if } i \text{ even} \end{cases} \\ a_{t(i)} &= \begin{cases} -\frac{2nV_{out}}{i\pi} & \text{if } i \text{ odd} \\ 0 & \text{if } i \text{ even} \end{cases} \end{aligned} \quad (7)$$

As the system in figure 5 is an LTI system, the current i_t can be calculated through

$$\begin{aligned} i_t &= \sum_{i=1}^{\infty} |G(ji\omega_s)| \{ a_{z(i)} \cos(i\omega_s t + \angle G(ji\omega_s)) \\ &\quad - a_{s4(i)} \cos(i\omega_s t - \varphi_{s4} + \angle G(ji\omega_s)) \\ &\quad - a_{t(i)} \cos(i\omega_s t - \varphi_{t1} + \angle G(ji\omega_s)) \\ &\quad + a_{t(i)} \cos(i\omega_s t - \varphi_{t2} + \angle G(ji\omega_s)) \}, \end{aligned} \quad (8)$$

where $G(ji\omega_s)$ is the transfer function from v_{lr} to i_t , i.e. the impedance, at the frequency $\frac{i\omega_s}{2\pi}$.

The transferred power is

$$\begin{aligned}
 p = & nV_{out} \sum_{i=1}^{\infty} \left\{ \frac{|G(ji\omega_s)|}{i\pi} 2 \sin\left(\frac{i\varphi_{t1} - i\varphi_{t2}}{2}\right) \right. \\
 & [a_{z(i)} \sin\left(\frac{i\varphi_{t1} + i\varphi_{t2}}{2} + \angle G(ji\omega_s)\right) \\
 & - a_{s4(i)} \sin\left(\frac{i\varphi_{t1} + i\varphi_{t2}}{2} - \varphi_{s4} + \angle G(ji\omega_s)\right) \\
 & - a_{t(i)} \sin\left(\frac{i\varphi_{t1} + i\varphi_{t2}}{2} - \varphi_{t1} + \angle G(ji\omega_s)\right) \\
 & \left. + a_{t(i)} \sin\left(\frac{i\varphi_{t1} + i\varphi_{t2}}{2} - \varphi_{t2} + \angle G(ji\omega_s)\right) \right\}. \quad (9)
 \end{aligned}$$

When the turns ratio n is increased the power that can be transferred through the converter increases too, but when increasing n above a certain value the reactive power grows as well, which results in higher device stresses and higher losses. Therefore the turns ratio is selected to be 14 to get an acceptable efficiency and on the other hand to get enough power in every possible converter state.

As mentioned above φ_{s4} , φ_{t1} and φ_{t2} can be selected independently. In the actual implementation $\varphi_{s4} = \pi$ and $\varphi_{t2} = \varphi_{t1} + \pi$ is selected. Independent of the modulation factor, which is defined through the machine's operating point, it is possible to control the power through variation of φ as shown in Figure 7. The output power is also slightly dependent on the machine's angle but this influence is small and it can be eliminated with the variation of φ too. It is worth noticing that for the given parameter values the maximum power that can be transferred from V_{in} to V_{out} (positive power) is higher than the power that can be transferred from V_{out} to V_{in} (negative power). In a normal dual active bridge for ideal conditions the positive and the negative maximum power are equal as stated in [11]. As the resistor in the conventional dual active bridge is quite small the reality matches the ideal equation quite well. For the motor we used, the zero phase resistance is significantly higher (see figure 17). Thus, the voltage drop across this resistance causes an unbalance in the maximums. Depending on the choice of n , V_{in} and V_{out} the positive or the negative power maximum is higher.

Figure 8 shows the actual controller. Other control schemes that use the other degrees of freedom will be described in future publications. There will be an analysis of the best choice of the degrees of freedom specified in table I.

Controller degrees of freedom:

- φ_{s4} : phase-shift angle of v_{s4}
- φ_{t1} : phase-shift angle of v_{t1}
- φ_{t2} : phase-shift angle of v_{t2}

Converter degrees of freedom:

- n : turns ratio

Table I: Degrees of freedom.

The model in figure 3b, where the machine model of figure 12 was inserted (which is explained in the next section), was

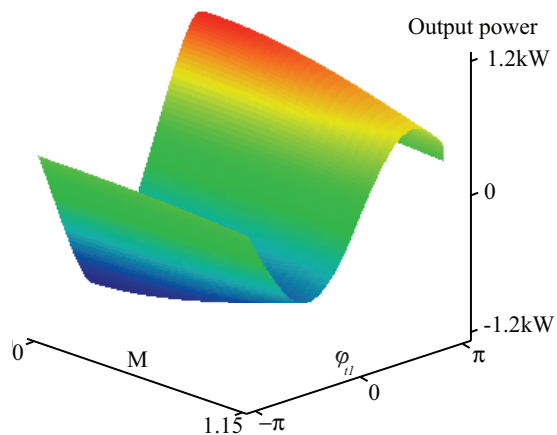


Figure 7: Power's dependency of φ and M for $n = 14$, $V_{in} = 400V$, $t = 0$ and $\varphi_{s4} = \pi$.

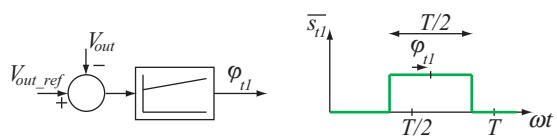


Figure 8: Output voltage control of the MFCS I.

simulated with the controller from figure 8. The load is a resistor. Figure 9 shows the simulation for the parameters given in table II. As can be seen, the output voltage and thus the output power is constant over the motor period. Furthermore, the voltage time product across the transformer is below the desired level and saturation is prevented.

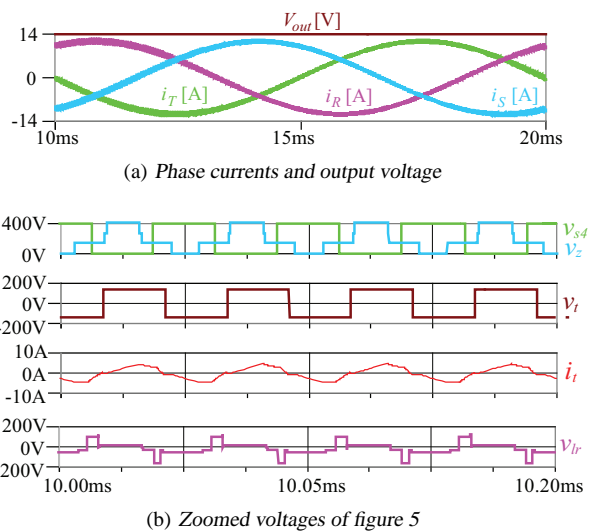


Figure 9: Simulation results for the MFCS-I with parameters given in table II.

In table III the characteristic values of the simulation are listed. As the zero sequence resistance of the actual machine is quite large, only an efficiency of about 70 percent is reached. Since the actual machine is not intended for the use in automotive applications, we measured an asynchronous motor

Parameter	Value
# poles p	8
motor speed	1500 rpm
switching frequency f	20 kHz
input voltage V_{in}	400 V
back EMF	102 Vrms
output voltage V_{out}	14 V
motor power	3 kW
converter output power	500 W
inductances	see table IV
resistances	see table IV
turn ratio n	14

Table II: Parameters of the MFCS.

that was used in a parallel hybrid car. The measurement shows that the impedance is significantly smaller. For a relevant machine like this the efficiency of the dc to dc converter is about 85 percents. Additionally, the efficiency can be increased by choosing a new control schema and including the other degrees of freedom specified in table I, as will be shown in future publications.

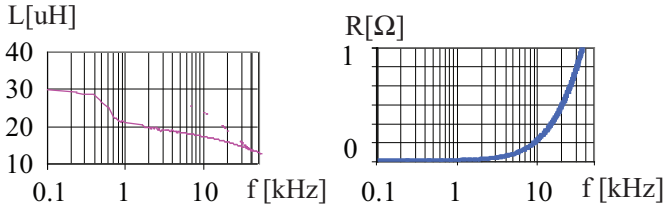


Figure 10: Zero phase inductance and resistance for a 50 kW motor.

Parameter	Value
$I_{R01,ms}$	0.538 A
$I_{R02,ms}$	0.310 A
$I_{R02,ms}$	0.727 A
$I_{R01,ms}$	0.331 A
$I_{t1,ms}$	32 A
$I_{s4,ms}$	2.3 A

Table III: Simulation results of the MFCS.

C. Detailed Flux Analysis of MFCS-I

The three voltages v_{P1} , v_{P2} and v_{P3} excite a magnetic flux in the machine. One part of this flux, called the main flux Ψ_m , is linked with all three phases. The other part of the flux, consisting of the slot leakage flux, the end winding leakage flux etc., is represented through the leakage flux Ψ_σ .

Figure 11a shows a COMSOL simulation for symmetrical, sinusoidal currents. Due to the spacial distribution the main fluxes of the individual windings sum up to zero if a zero-sequence current flows through the machine (see figure 11b).

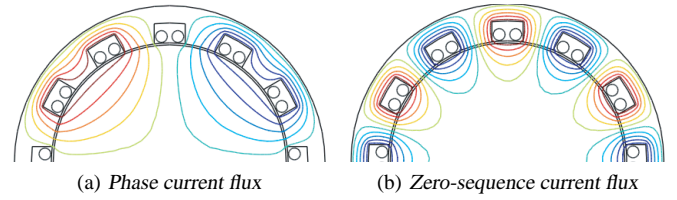


Figure 11: COMSOL simulation of the magnetic flux for (a) symmetrical, sinusoidal currents and (b) zero-sequence current.

This means that a zero-sequence current excites only a leakage flux.

Although the local flux is influenced by the zero sequence current, the total torque is not. Because of the spacial distribution of the zero-sequence current, the forces cancel to zero, so the total torque of a machine with zero sequence current is equal to the one of a machine without zero sequence current.

To model these effects, the equivalent motor circuit depicted in figure 12 is used.

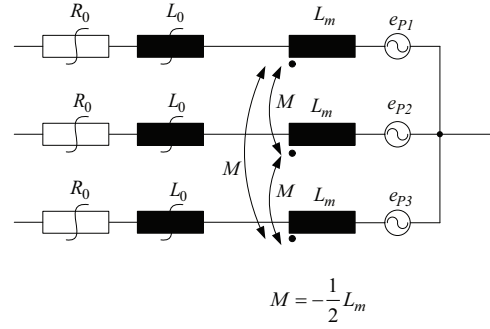


Figure 12: Simplified equivalent circuit of the motor.

As the losses due to skin and proximity effect and the core losses are frequency dependent, the resistance R_0 also changes with the frequency. The same applies to the inductance L_0 . Figure 13 shows the four-step R-L ladder circuit for modelling the frequency dependence of the zero-sequence impedance of the machine shown in figure 17.

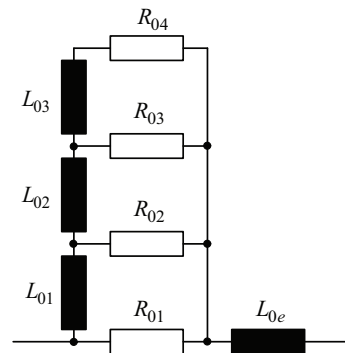


Figure 13: Equivalent circuit representing the frequency dependent R_0 and L_0 in figure 5.

Parameter	Value
L_{0e}	1.0132 mH
R_{01}	150.29 Ω
L_{01}	0.60183 mH
R_{02}	32.252 Ω
L_{02}	0.2094 mH
R_{03}	6.921 Ω
L_{04}	72.861 μ H
R_{04}	1.4852 Ω

Table IV: Parameters for the equivalent circuit in figure 5.

It is clear that the mutual inductances are frequency dependent too, but as for the dc-dc converter only the zero phase current is relevant, this effect is omitted in our equivalent circuit.

D. Design and Experimental Results of MFCS-I

To verify the functionality of the proposed MFCS-I, a synchronous motor with accessible star point (and integrated secondary windings in order to also allow the evaluation of MFCS-II) with the parameters given in table V has been designed. Figure 14 shows the motor with the extra windings as described in the next section.

Parameter	Value
# poles	8
nominal speed	1500 rpm
input voltage V_{in}	250 V...400 V
motor power	3 kW
back EMFs e_R, e_S and e_T	67.8 Vrms at 1000 rpm

Table V: Parameters of the prototype.

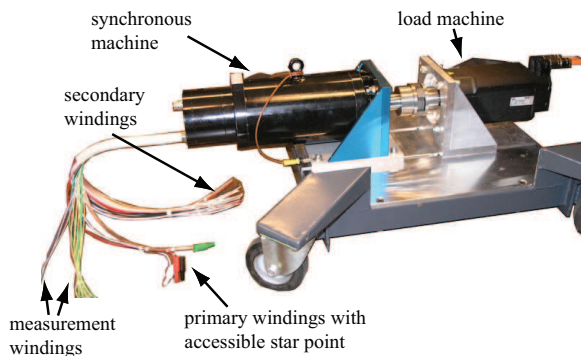


Figure 14: 3 kW permanent magnet synchronous motor with accessible star point and secondary windings for MFCS-II.

The motor is driven by the 6.8 kW three phase back-to-back converter. The output stage, fed with an external dc-link voltage, is used to drive the motor. One leg of the input stage serves as the fourth leg in figure 3b).

The output rectifier in figure 15 was designed for an output power of 1 kW.

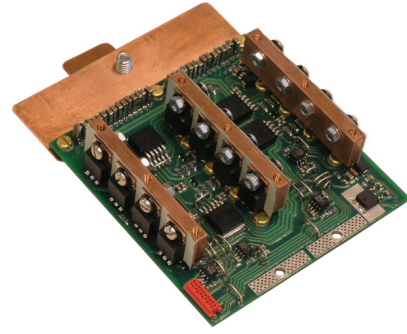


Figure 15: Active secondary side rectifier.

The results of the zero-sequence voltage measurement in figure 16 and the simulation in figure 4b match very well. The measurement of the phase inductance $L_p = L_m + L_\sigma$ and the zero sequence inductance $\frac{L_\sigma}{3}$ show the large zero sequence resistance, but as already stated this problem will disappear as in hybrid cars machines with lower resistances are used (see figure 10).

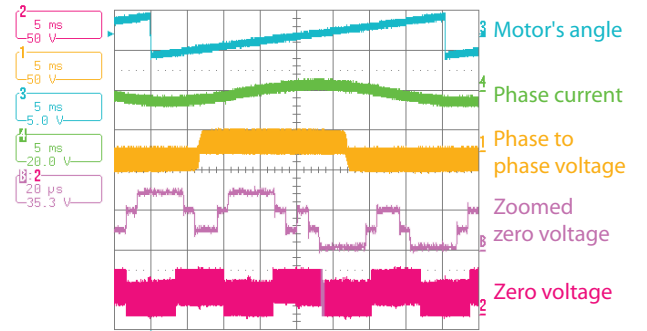


Figure 16: Measurement of the zero-sequence voltage for a modulation index of $M = 0.5$ and an input voltage $V_{in} = 50$ V.

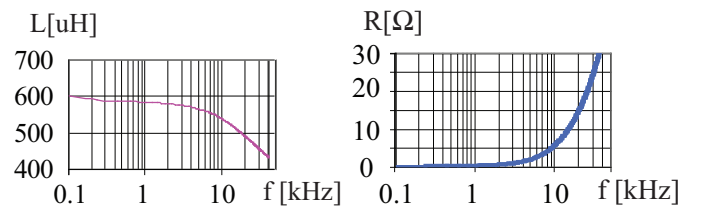


Figure 17: Zero phase inductance and resistance of the synchronous motor (figure 14).

III. MFCS-II

In a second integration step the galvanic isolation of V_{out} can also be integrated into the motor (see figure 3c) in order to reduce the costs and the weight further. To do so, additional windings must be placed in the slots together with the conventional winding.

A. Basic Principle of Operation MFCS-II

Figure 18 shows a simplified sketch of the integration of the transformer proposed for the MFCS-II. The conventional

motor windings act as the primary windings of the three transformers. The additional windings are forming the secondary ones. The machine stator iron is used as magnetic core. As the machine has 120 primary turns per pole pair and the winding geometry allows not less than 12 secondary windings per phase, the secondary windings of the four pole pairs will be connected in series while the primaries are connected in parallel. So the desired turn ratio of 14 (as explained in subsection IIA) is achieved. Additionally, there is one measurement winding per slot to prove if the COMSOL simulations match with the actual fluxes.

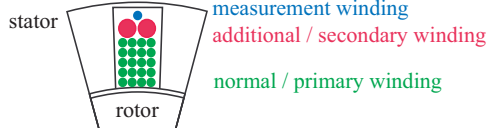


Figure 18: Transformer integrated into the motor.

If there is a voltage applied to phase $P1$, a flux Ψ_{P1} begins to build up, inducing a voltage v_{P1_2} in the secondary winding $P1_2$ proportional to v_{P1_1} (ignoring losses). The same applies to phases $P2$ and $P3$. If the secondary windings are connected in series, the voltage appearing on the secondary side is without load just $v_2 = \frac{1}{n}(v_z - v_{s4})$ as the remaining voltages cancel to zero. If a load is connected to the secondary side, the voltage is slightly changed because of the losses and the reactive voltage drop (see figure 19, v_{2load}). Again an active rectifier is used to obtain the desired dc voltage V_{out} . The control can be implemented in a similar way as for MFCS-I.

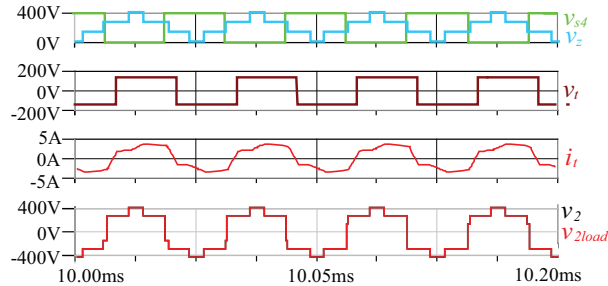


Figure 19: Simulation results for the MFCS-II with parameters given in table II.

Figure 19 shows the simulation for figure 3b with the parameters given in table II. The phase currents and the output voltage are similar to figure 9a so they are not depicted here,

but again, the output power is constant over the motor period.

IV. CONCLUSION

By integrating the dc-dc converter, which interfaces the low and the high voltage buses of a hybrid vehicle. In this paper, two new concepts for integrating the converter are presented and verified by simulations. With the first concept MFCS-I, the inverter and the machine are used to implement a primary bridge leg of an isolated full bridge dc-dc converter. In the second concept MFCS-II, the transformer is additionally integrated into the machine so that only one auxiliary bridge leg and a secondary rectifier are required to realize an isolated dc-dc converter.

In a next step, the hardware for the MFCS-I and the MFCS-II are taken into operation and the simulations are verified. Further different control schemes with the degrees of freedom described in table I are analyzed.

REFERENCES

- [1] A. Emadi, M. Ehsani, J.M. Miller, "Advanced Silicon Rich Automotive Electrical Power Systems," Proc. 18th Digital Avionics Systems Conference, St. Louis, Missouri, Oct. 1999.
- [2] K. Moriya, H. Nakai, Y. Inaguma, H. Ohtani, S. Sasaki, "A Novel Multi-Functional Converter System Equipped with Input Voltage Regulation and Current Ripple Suppression," Industry Applications Conference, 2005. Fourtieth IAS Annual Meeting. Conference Record of the 2005.
- [3] Seung-Ki Sul, Sang-Joon Lee, "An Integral Battery Charger for Four-wheel Drive Electric Vehicle," IEEE Transactions on Industry Applications, Vol. 31, No. 5, September/October 1995.
- [4] Bayerische Motoren Werke AG, "Switching Device for Linking Various Electrical Voltage Levels in a Motor Vehicle," European Patent WO 2006/105840 A1.
- [5] Shigenori Kinoshita, Koetsu Fujita, Junichi Ito; Fuji Electric Co. "Electric System for Electric Vehicle," United States Patent 6,066,928.
- [6] Shoichi Sasaki; Toyota Jidosha Kabushiki Kaisha "Multiple Power Source System and Apparatus, Motor Driving Apparatus, and Hybrid Vehicle with Multiple Power Source System Mounted Thereon," United States Patent 6,476,571 B1.
- [7] D.S. Carlson, C.C. Stancu, J.M. Nagashima, S. Hiti, K.M. Rahman; General Motors Corporation "Auxiliary Power Conversion by Phase-Controlled Rectification," United States Patent 6,617,820 B2.
- [8] C.C. Stancu, S. Hiti, J. Nagashima; General Motors Corporation "Auxiliary Power Conversion for an Electric Vehicle Using High Frequency Injection into a PWM Inverter," United States Patent 6,262,896 B1.
- [9] ETH Zurich, "Drehstromantriebssystem mit motorintegriertem Hochfrequenztrafo zur bidirektionalen Kopplung der Versorgungsspannungen," Schweizerische Patentanmeldung, July 27, 2006.
- [10] ETH Zurich, "Drehstromantriebssystem mit hochfrequent potentialgetrennter bidirektionaler Kopplung der Versorgungsspannungen," Schweizerische Patentanmeldung, July 27, 2006.
- [11] M.H. Kheraluwala, R.W. Gascoigne, D.M. Divan, E.D. Baumann, "Performance Characterization of a High-Power Dual Active Bridge dc-to-dc Converter," Power Electronics in Transportation, pp. 39-44, Oct. 2002.